Elastic imaging conditions based on Helmholtz decomposition

Zaiming Jiang, John C. Bancroft, and Laurence R. Lines

ABSTRACT

This report demonstrates Helmholtz decomposition performed on particle velocity wavefields with a staggered-grid FD scheme. In addition, Helmholtz decomposition is used in elastic reverse-time migration, and PP, PS, SP, and SS images are obtained.

INTRODUCTION

Multicomponent seismic data can be separated into P and S modes by Helmholtz decomposition. The decomposition can be done on the surface or in the subsurface (Yan and Sava, 2007). Usually, the decomposition is performed on displacement and body force vectors in geophysics.

There are two categories of elastic imaging conditions. One is based on multiple components of displacements or particle velocities. The other category of elastic imaging conditions is based on wave modes (P and S).

There is a rich literature on elastic imaging based on Helmholtz decomposition. Two examples are by Yan and Sava (2007) and Du et al. (2012). Yan and Sava (2007) presented a 2D imaging method based on displacement decomposition. Only PP and PS images were shown. While Du et al. (2012) presented a PS wave imaging method in 3D.

This report shows that Helmholtz decomposition can be implemented on particle velocity wavefields, and it can be done with a staggered-grid FD scheme. The decomposition is performed on subsurface wavefields. Further more, the report presents imaging conditions based on Helmholtz decomposition, and shows PP, PS, SP, and SS images obtained.

WAVEFIELD HELMHOLTZ DECOMPOSITION

Helmholtz decomposition of particle velocity wavefields

Similar to the Helmholtz decomposition of displacement or body force (Aki and Richards, 2002, chap. 4), particle velocity wavefield decomposition can be written as

$$\boldsymbol{v} = \nabla\phi + \nabla \times \boldsymbol{\psi}, \tag{1}$$

where $\boldsymbol{v}$ denotes the particle velocity vector, ϕ is the Helmholtz potential scalar for P mode, and $\boldsymbol{\psi}$ is the Helmholtz potential vector for S mode.

Using Φ and $\boldsymbol{\Psi}$ to denote divergence and curl of the particle velocity, one gets

$$\Phi = \nabla \cdot \boldsymbol{v} = \nabla^2\phi, \tag{2a}$$

$$\boldsymbol{\Psi} = \nabla \times \boldsymbol{v} = \nabla \times \nabla \times \boldsymbol{\psi}. \tag{2b}$$

Thus, Φ and $\boldsymbol{\Psi}$, respectively, describe the Helmholtz potentials for P and S modes as well. Note that Φ is a scalar while $\boldsymbol{\Psi}$ is a vector.
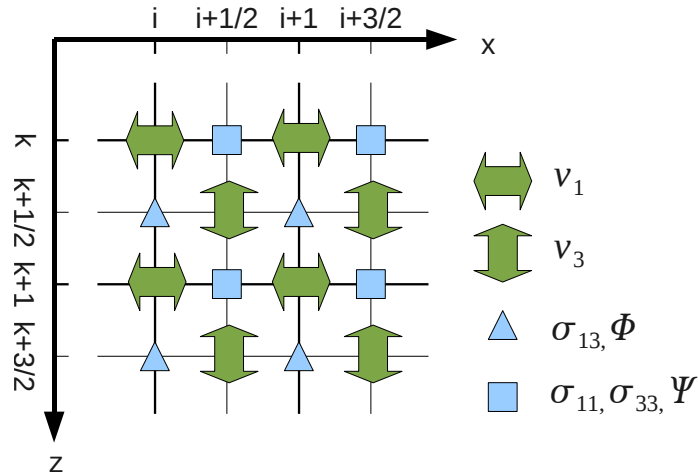
FIG. 1: A staggered grid for 2D P-SV wave modelling and wave mode decomposition.

2D FD approximation with a staggered-grid FD scheme

2D FD approximations of Equation 2 can be derived for the P-SV case. In a 2D P-SV case of a (x_1, x_3) coordinate system, the vector $\boldsymbol{\Psi}$ has only one component pointing in the direction of x_2, so one may use a scalar Ψ, referred to as a scalar curl (Marsden and Tromba, 2003), to denote the vector $\boldsymbol{\Psi}$ without causing any confusion. On a staggered-grid scheme shown in Figure 1, from the definitions of divergence and curl one can derive the following approximations

$$\Phi_{i+1/2,k} = \frac{v_{1i+1,k} - v_{1i,k}}{h} + \frac{v_{3i+1/2,k+1/2} - v_{3i+1/2,k-1/2}}{h}, \tag{3a}$$

$$\Psi_{i,k+1/2} = \frac{v_{1i,k+1} - v_{1i,k}}{h} - \frac{v_{3i+1/2,k+1/2} - v_{3i-1/2,k+1/2}}{h}, \tag{3b}$$

where v_1 and v_3 are, respectively, horizontal and vertical components of particle velocities, and h is a FD space step. Thus, P and S modes of particle velocity wavefields can be obtained from two components of the wavefields.

In order to verify the correctness of the above FD approximation, an elastic modelling experiment is designed, and wave decomposition is accomplished using the modelled wavefields.

First, an elastic wave modelling experiment is carried out. The modelling method is based on the one by Virieux (1986). The subsurface model includes three sets of parameters: density and Lamé constants. The corresponding P-wave velocity model, which is more straightforward for people than density or Lamé constants models, is shown in Figure 2a. A time step of $0.0001s$ and a space step of $1m$ are used. A P-wave source is put at $(650m, 400m)$. Horizontal and vertical component snapshots of the particle velocity wavefields at time $0.15s$ are, respectively, shown in Figure 2b and 2c. Five wavefronts in the wavefields are expected and recognizable in both components: a direct P wave generated from the energy source, a PP reflection upon the rock interface at $500m$, a corresponding PS reflection, a PP transmitted event under the rock interface, and a corresponding PS transmitted event.

Then, 2D approximation of Helmholtz decomposition, Equation 3, is applied to the modelled wavefield components. For the components shown in Figure 2b and 2c, the separated wave P and S modes are, respectively, shown in Figure 2d and 2e.

ELASTIC IMAGING USING HELMHOLTZ DECOMPOSITION

Similar to source-normalized cross-correlation imaging conditions based on displacements (Whitmore and Lines, 1986; Kaelin and Guitton, 2006; Chattopadhyay and McMechan, 2008) or particle velocities (Jiang, 2012), source-normalized cross-correlation imaging conditions using P- and S-mode potentials can be written as

$$I_{PP}(x_1, x_3) = \frac{\sum_t \Phi_s(x_1, x_3, t)\Phi_r(x_1, x_3, t)}{\sum_t \Phi_s^2(x_1, x_3, t)}, \tag{4a}$$

$$I_{PS}(x_1, x_3) = \frac{\sum_t \Phi_s(x_1, x_3, t)\Psi_r(x_1, x_3, t)}{\sum_t \Phi_s^2(x_1, x_3, t)}, \tag{4b}$$

$$I_{SP}(x_1, x_3) = \frac{\sum_t \Psi_s(x_1, x_3, t)\Phi_r(x_1, x_3, t)}{\sum_t \Psi_s^2(x_1, x_3, t)}, \tag{4c}$$

$$I_{SS}(x_1, x_3) = \frac{\sum_t \Psi_s(x_1, x_3, t)\Psi_r(x_1, x_3, t)}{\sum_t \Psi_s^2(x_1, x_3, t)}, \tag{4d}$$

where $I_{PP}(x_1, x_3)$ represents the image component produced by P modes of the source and receiver wavefields, $I_{PS}(x_1, x_3)$ represents the image component produced by P modes of the source and S modes of the receiver wavefields, etc.

Following an elastic RTM workflow described by Jiang (2012), using Helmholtz decomposition and imaging conditions described above, elastic RTM images are obtained (Figure 3).

CONCLUSIONS

Helmholtz decomposition is implemented on particle velocity wavefields with a staggered-grid FD scheme. Elastic imaging based on the Helmholtz decomposition in the staggered-grid scheme is also achievable.

ACKNOWLEDGEMENTS

REFERENCES

Aki, K., and Richards, P. G., 2002, Quantitative Seismology: Theory and Methods: University Science Books.

Chattopadhyay, S., and McMechan, G. A., 2008, Imaging conditions for prestack reverse-time migration: Geophysics, **73**, No. 3, S81–S89.

Du, Q., Gong, X., Zhu, Y., Fang, G., and Zhang, Q., 2012, Ps wave imaging in 3d elastic reverse-time migration: SEG Las Vegas 2012 Annual Meeting Expanded Abstract.

(a) A two-layer subsurface model

(b) Horizontal component

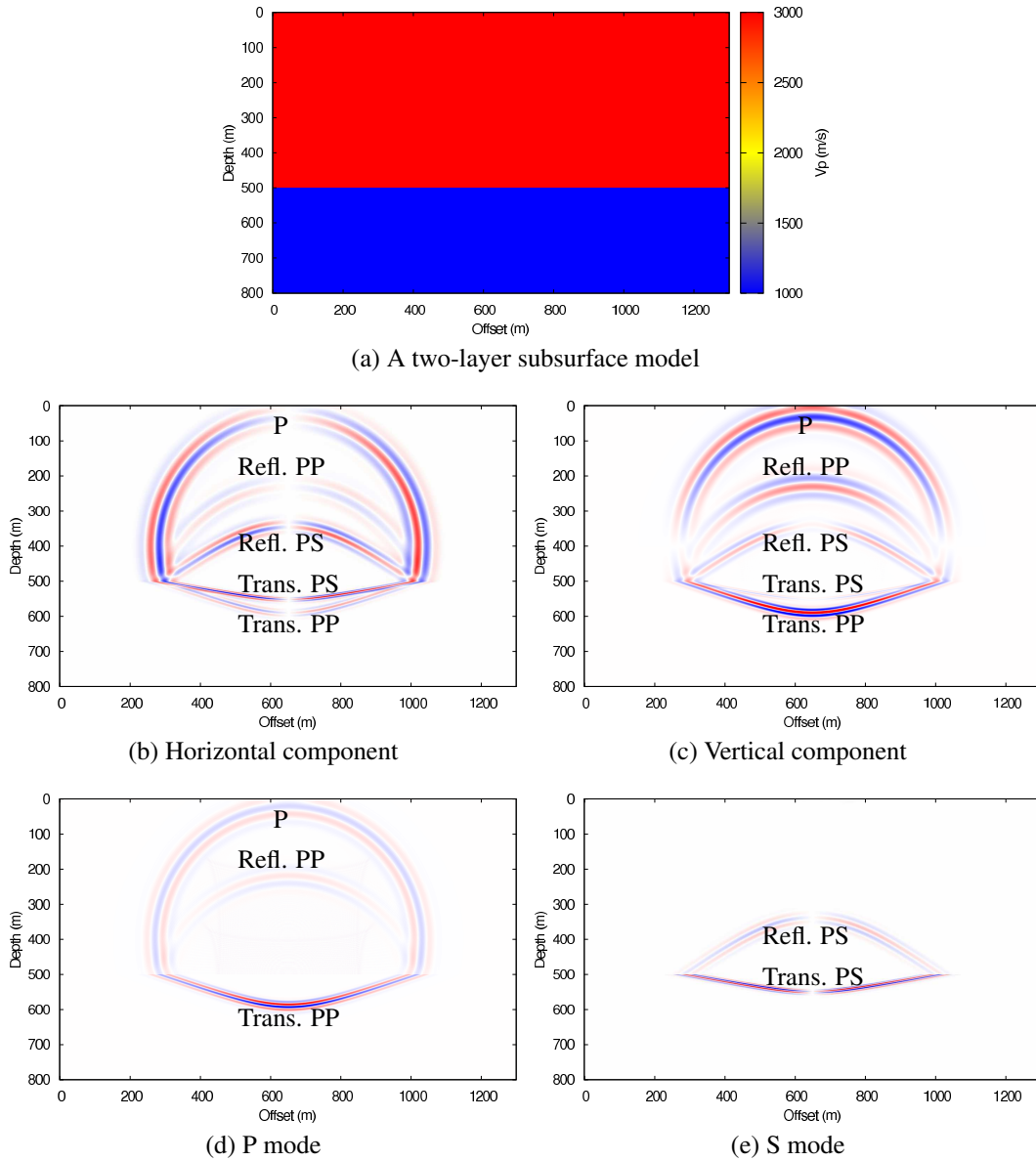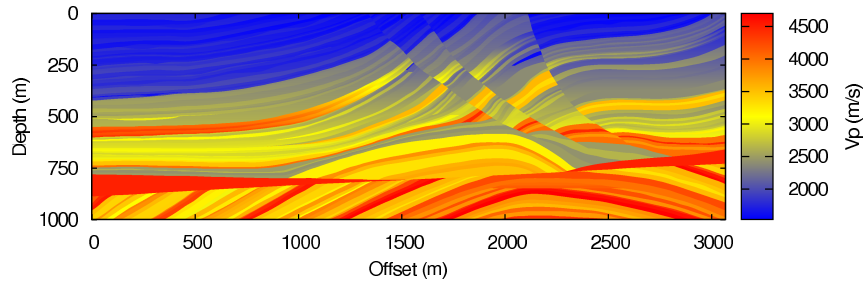(c) Vertical component

(d) P mode

(e) S mode

FIG. 2: Two components of a wavefield is decomposed into P and S modes. (a) is P-wave velocities of an elastic subsurface model. (b) and (c) are two components of a particle velocity wavefield modelled with a P-wave source at (650m, 400m) in (a), (d) and (e) are P and S modes obtained from (b) and (c) by Helmholtz decomposition approximations (Equation 3).
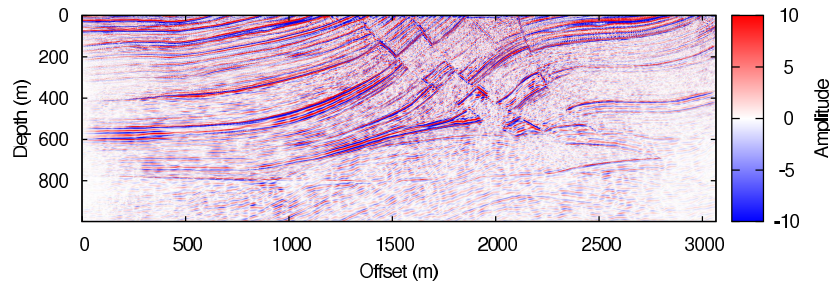
(a) P-wave velocities of shrunk Marmousi2
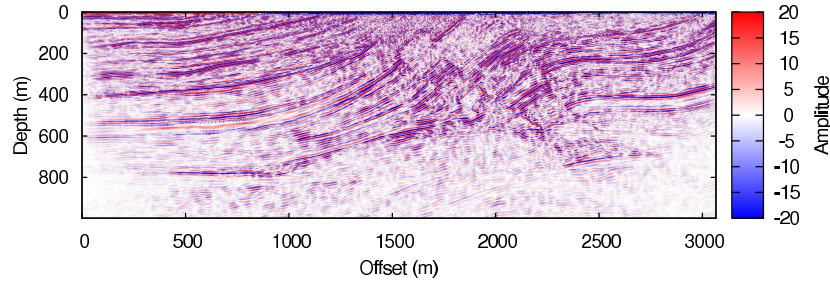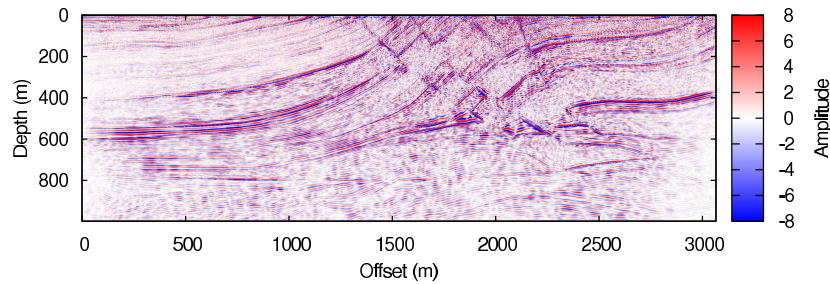

(b) PP (Equation 4a)
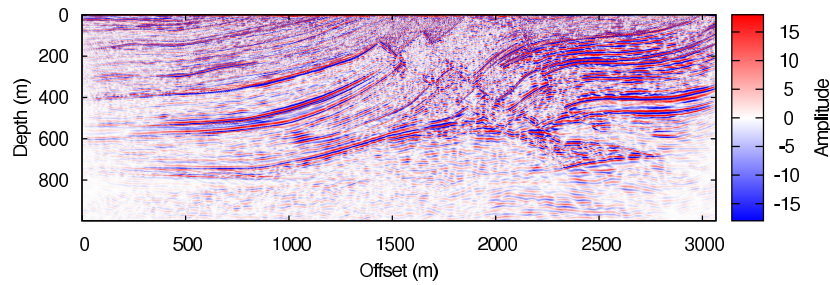
(c) PS (Equation 4b)

(d) SP (Equation 4c)

(e) SS (Equation 4d)

FIG. 3: P-wave velocities of shrunk Marmousi2 (a) and elastic RTM images (b, c, d, and e) based on Helmholtz decomposition.

Jiang, Z., 2012, Elastic wave modelling and reverse-time migration by a staggered-grid finite-difference method: Ph.D. thesis, The University of Calgary.

Kaelin, B., and Guitton, A., 2006, Imaging condition for reverse time migration: SEG Eightieth Annual Meeting Expanded Abstract, 2594–2598.

Marsden, J. E., and Tromba, A. J., 2003, Vector calculus: W H Freeman and Company.

Virieux, J., 1986, P-SV wave propagation in heterogeneous media: Velocity-stress finite-difference method: Geophysics, **51**, No. 4, 889–901.

Whitmore, N., and Lines, L., 1986, Vertical seismic profiling depth migration of a salt-dome flank: Geophysics, **51**, No. 5, 1087–1109.

Yan, J., and Sava, P., 2007, Elastic wavefield imaging with scalar and vector potentials: SEG San Antonio 2007 Annual Meeting Expanded Abstract, 2150–2154.